16 October 2000

PHYSICS LETTERS A

ELSEVIER

Physics Letters A 275 (2000) 254–259

www.elsevier.nl/locate/pla

Experimental observation of dynamic stabilization in a double-well Duffing oscillator

Youngtae Kim [a,*], Sang Yeol Lee [a], Sang-Yoon Kim [b]

[a] *Department of Molecular Science and Technology, Ajou University, Suwon, Kyunggi-Do 442-749, South Korea*
[b] *Department of Physics, Kangwon National University, Chunchon, Kangwon-Do 200-701, South Korea*

Received 1 May 2000; accepted 29 August 2000
Communicated by A.R. Bishop

Abstract

Dynamic stabilization of an unstable periodic orbit, a new interesting non-equilibrium phenomenon in driven nonlinear systems, has been experimentally observed in an electronic analog circuit of a driven double-well Duffing oscillator. We suggest that the dynamic stabilization is a generic property of driven nonlinear systems with humped potentials. © 2000 Published by Elsevier Science B.V.

PACS: 05.45.-a

Since the discovery of chaos in the Lorentz equation [1], investigations of nonlinear dynamical systems have been an active research subject. As a result, enormous progresses have been made in understanding various types of bifurcations, routes to chaos, etc. Good examples of nonlinear dynamical systems showing many interesting dynamical behaviors are driven nonlinear systems such as driven nonlinear oscillators. Dynamics of the driven nonlinear oscillators is governed by the equation,

$$\ddot{x} + \gamma\dot{x} - f(x) = A\sin(\omega t), \tag{1}$$

where $f(x) = -dV(x)/dx$ is a nonlinear force, $V(x)$ is an anharmonic potential function, γ is a damping factor, $A\sin(\omega t)$ is a driving force with amplitude A and frequency ω, and the overdot denotes a differentiation with respect to time t. Typical examples of the driven nonlinear oscillators are the driven pendulum [2], Toda oscillator [3], and Duffing oscillator [4–14]. Dependence of dynamical properties of the driven nonlinear oscillators, such as bifurcations and chaos, on A and ω has been investigated extensively by many researchers [2–14].

For the symmetric Duffing oscillator, the potential function $V(x)$ can be expressed as follows:

$$V(x) = \frac{a}{2}x^2 + \frac{b}{4}x^4, \tag{2}$$

where a and b are constants. Here we consider only the bounded case with positive b ($b > 0$). Then, depending on the sign of a, the potential function becomes one of two different types: double-well potential for $a < 0$ or single-well potential for $a > 0$. For the Duffing oscillator with a double-well poten-

* Corresponding author.
E-mail addresses: ytkim@madang.ajou.ac.kr (Y. Kim), sykim@cc.kangwon.ac.kr (S.-Y. Kim).

0375-9601/00/$ - see front matter © 2000 Published by Elsevier Science B.V.
PII: S0375-9601(00)00572-7

tial, there are two stable equilibrium points at $x = \pm\sqrt{-a/b}$ and one unstable equilibrium point at $x = 0$. On the contrary, the Duffing oscillator with a single well has only a stable equilibrium point at $x = 0$. Phase diagrams on the ω–A plane, chaos, bifurcation diagrams, coexisting multiple attractors, hysteresis, and crisis are among the dynamical properties of the driven double-well and single-well Duffing oscillator which have been studied by many authors [4–14].

The driven nonlinear oscillator in Eq. (1) is a dissipative dynamical system, meaning that oscillations are maintained by continuous energy input from an external source. It is well known that various interesting non-equilibrium phenomena arise in the nonlinear dissipative systems with continuous energy input. Pattern formation in the spatially extended nonlinear dissipative systems such as fluid, chemical, and granular systems [15] is one of non-equilibrium phenomena which cannot be observed in conservative systems.

In this Letter, we have experimentally demonstrated a new interesting non-equilibrium phenomenon in the double-well Duffing oscillator: *dynamic stabilization* of an unstable symmetric periodic orbit arising from the unstable equilibrium point. We show that, as the amplitude A of the driving force passes through a threshold value, the unstable symmetric periodic orbit becomes stabilized via a reverse supercritical pitchfork bifurcation by absorbing a pair of stable asymmetric periodic orbits. After this dynamic stabilization, the double-well Duffing oscillator behaves as the single-well Duffing oscillator, because the central barrier of the potential gives no significant effect on the motion of the system. Finally, we suggest that the dynamic stabilization is a rather general phenomenon occurring in many driven nonlinear systems with humped potentials which provide both the stable and unstable equilibrium points.

Here we consider the case of $a = -1$ and $b = 1$ in the double-well potential $V(x)$ without loss of generality. Then, for the unforced case of $A = 0$, there exist a saddle equilibrium point at $x = 0$ and a conjugate pair of stable equilibrium points at $x = \pm 1$. However, as A is increased from 0, one symmetric saddle-type orbit and two asymmetric stable orbits with the same period $2\pi/\omega$ arise from the saddle equilibrium point and the two stable equilibrium points of the potential, respectively [6,7]. We also note that they become the fixed points of the Poincaré map P, generated by stroboscopically sampling the orbit points with the external driving period $T\ (= \omega/2\pi)$. Hereafter, the symmetric saddle fixed point and the asymmetric stable fixed points will be denoted by z_s^* and z_a^*, respectively.

For the experimental study, we built an analog electronic circuit of the double-well Duffing oscillator for a moderately damped case of $\gamma = 0.1$ with the conventional operational amplifier and multiplier IC's [14]. Using this analog simulator driven by the synthesizer/function generator (HP 3325B), we made an analog study and thus observed dynamic stabilization experimentally. For clear presentation of the dynamic stabilization, the bifurcation diagram (plot of x versus A) and the phase-flow and Poincaré-map plots are given. As known well, the bifurcation diagram and the Poincaré map can be easily obtained through a stroboscopic sampling of the values of $(x, \dot{x})$ with the external driving period T (the sampling phase is fixed at the maxima of the driving force). To confirm and complement the experimental results, a numerical study was also carried out [16]. Linear stability of a fixed point of the Poincaré map can be numerically determined from the eigenvalues, called the Floquet multipliers, of the linearized Poincaré map DP, which can be obtained using the Floquet theory [17]. Since the Poincaré map P has a constant Jacobian determinant (det) less than unity ($\det DP = e^{-\gamma T}$), the only possible bifurcations of the fixed points are the saddle-node (SN), pitchfork (PF), and period-doubling (PD) bifurcations. When a Floquet multiplier passes through 1, a PF or SN bifurcation takes place. On the other hand, when it passes through -1, a PD bifurcation occurs.

By varying the two parameters A and ω, we experimentally investigated the bifurcation behavior associated with stability of the symmetric and asymmetric fixed points z_s^* and z_a^* of the Poincaré map in the range of $2.2 < \omega < 4.0$. Fig. 1 shows the associated bifurcation structure in the ω–A plane. The symbols PF and SN in Fig. 1 represent the pitchfork and saddle-node bifurcation curves for the symmetric fixed point z_s^*, while the symbol PD denotes the period-doubling bifurcation curve for the asymmetric fixed points z_a^*. These bifurcation curves

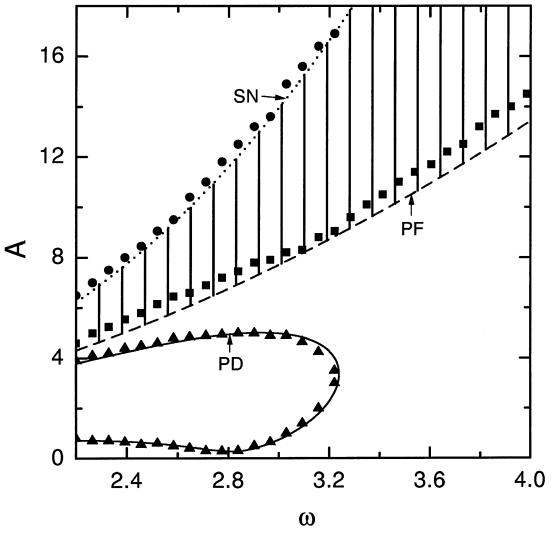

Fig. 1. Phase diagram of a driven Duffing oscillator with a double-well potential with $a=-1$ and $b=1$ for a moderately damped case of $\gamma=0.1$. The symbols PF, SN and PD denote the pitchfork, saddle-node, and period-doubling bifurcation curves, respectively. The experimental data for the PF, SN, and PD curves are represented by the squares, circles, and triangles, respectively, while the numerical data for them are denoted by the dashed, dotted, solid lines, respectively. The hatched region with the vertical lines is just the stability of the unstable symmetric, arising from the unstable equilibrium point of the potential. For other details, see the text.

were experimentally obtained by both amplitude and frequency scanning starting from high ω to low ω. The experimental data for the PF, SN, and PD curves are denoted by the squares, circles, and triangles, respectively. The data obtained through numerical calculations are also given for a comparison with the experimental results. The numerical data for the PF, SN, and PD curves are denoted by the dashed, dotted, and solid lines, respectively. Note that the experimental results agree quite well with the numerical results.

The region, hatched with the vertical lines, in Fig. 1 is just the stability region of the symmetric saddle fixed point z_s^*, arising from the unstable equilibrium point of the potential. It is bounded by a lower PF curve and by an upper SN curve. When crossing the PF curve, the symmetric saddle fixed point z_s^* becomes stabilized through a reverse supercritical PF bifurcation by absorbing a pair of stable asymmetric fixed points z_a^*, arising from the stable equilibrium points of the potential. As a result of this dynamic stabilization, a symmetric stable orbit with period $2\pi/\omega$ (fixed point for the Poincaré map), encircling the unstable equilibrium point of the potential, appears. This stabilized symmetric orbit corresponds to the stable symmetric orbit, arising from the stable equilibrium point of the potential in the single-well Duffing oscillator. It means that the dynamical behavior of the double-well Duffing oscillator after such a dynamical stabilization becomes essentially the same as that of the single-well Duffing oscillator [4,5]. However, such stabilized symmetric orbit disappears via a SN bifurcation at the upper SN curve.

We now present the concrete examples of the bifurcations associated with dynamic stabilization of the symmetric saddle fixed point. Before proceeding further, note that the PD bifurcation curve for the asymmetric fixed points z_a^* is folded back at $\omega=\omega_f$ ($\simeq 3.25$) (see Fig. 1). Hence, we first consider the simplest case of $\omega>\omega_f$, where no PD bifurcations occur. Fig. 2(a) shows the multi-exposured picture of the bifurcation diagram for $\omega=3.3$ taken by both forward and backward amplitude scanning. As clearly shown there, the two asymmetric stable fixed points z_a^*, arising from the stable equilibrium points at $x=\pm 1$, merge through a reverse PF bifurcation for $A\simeq 9.1$, and then a symmetric orbit, encircling the unstable equilibrium point at $x=0$, appears. This indicates the dynamic stabilization. However, such a stabilized symmetric orbit disappears for $A\simeq 17.8$ through a SN bifurcation, and then a jump to a large symmetric orbit, encircling all the three equilibrium points of the potential, takes place, which is denoted by a broken arrow. We also followed the large symmetric orbit by backward amplitude scanning and found that it disappears for $A\simeq 1.2$ via a SN bifurcation. Thus a large hysteresis occurs.

For $\omega<\omega_f$, the mechanism of dynamic stabilization is the same, except for the bifurcation behavior of the asymmetric fixed point z_a^*. Fig. 2(b) shows the bifurcation diagram for $\omega=3.2$. As shown there, the asymmetric fixed points z_a^* become unstable for $A\simeq 1.9$ via PD bifurcations. However, they become restabilized for $A\simeq 4.3$ via reverse PD bifurcations. Note that the subsequent bifurcations, associated with the dynamic stabilization, are the same as those for the above case of $\omega=3.3$.

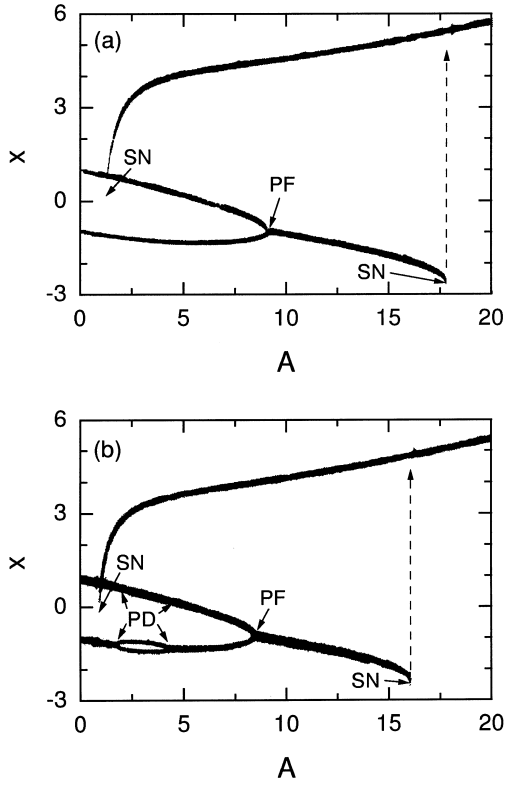

Fig. 2. Multi-exposured pictures of the bifurcation diagrams for (a) $\omega = 3.3$ and (b) $\omega = 3.2$. Here the symbols PF, SN and PD denote the same as those in Fig. 1. The stable asymmetric orbits merge into the stable symmetric orbit through a reverse PF bifurcation. However, the stabilized symmetric orbit also disappears via a SN bifurcation, and then jumps to a large symmetric orbit, which is indicated by the broken arrow. For other details, see the text.

The process of the dynamic stabilization of the unstable symmetric orbit can be more clearly understood by observing the change in the phase portraits of the stable asymmetric orbits and the unstable symmetric orbit. Figs. 3(a)–(c) show the double-exposed pictures of the phase portraits for $\omega = 3.3$ taken in the experiment. As A is increased, the two stable asymmetric orbits, arising from the stable equilibrium points at $x = \pm 1$, become larger and closer as shown in Figs. 3(a) and (b), and eventually they merge. After that, a stable symmetric orbit, encircling the unstable equilibrium point at $x = 0$, appears [see Fig. 3(c)]. Thus, dynamic stabilization of the unstable symmetric orbit, arising from the unstable equilibrium point of the potential, occurs. However, unfortunately, the symmetric orbit before the dynamic stabilization cannot be observed experimentally, because it is unstable. To confirm and complement the experimental results, we also made a numerical study for the same values of the parameters. As shown in Figs. 3(d) and (e), with increasing A, the central unstable symmetric orbit, denoted by a dashed line, becomes larger and closer to the two stable asymmetric orbits, denoted by a solid line. Eventually, it becomes stabilized by absorbing the two asymmetric stable orbits via a reverse supercritical PF bifurcation. A stabilized symmetric orbit is shown in Fig. 3(f).

We now discuss the dynamical behavior after the dynamic stabilization of the unstable symmetric orbit. Note that the stabilized symmetric orbit, encir-

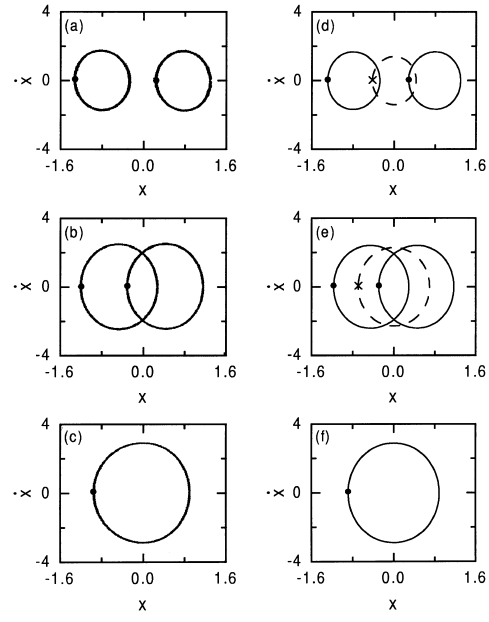

Fig. 3. Phase portraits of the symmetric and asymmetric orbits associated with the dynamic stabilization for $\omega = 3.3$. The phase portraits in the left column are obtained through an analog simulation, while those in the right column are obtained through a numerical computation. The values of the driving amplitude are $A = 5$ in (a) and (d), $A = 8$ in (b) and (e), and $A = 10$ in (c) and (f). The phase flow and the Poincaré map for a stable orbit are denoted by a solid line and a circle, respectively, while those for an unstable orbit are represented by a dashed line and a cross. With increasing A the asymmetric orbits become larger, and move toward each other. Eventually, they merge into a symmetric orbit, encircling the unstable equilibrium point of the potential. For other details, see the text.

cling the unstable equilibrium point of the potential, corresponds to the stable symmetric orbit, arising from the stable equilibrium point in the single-well Duffing oscillator. Hence, the double-well Duffing oscillator behaves as the single-well Duffing oscillator, because the central potential barrier gives no significant effect on the dynamics of the system. As an example, a bifurcation diagram, obtained by frequency scanning for $A = 10$, is given in Fig. 4(a). As ω decreases through a threshold value, the stabilized symmetric orbit disappears via a SN bifurcation, and then a jump to a large symmetric orbit, encircling all the three equilibrium points of the potential, occurs. A phase portrait of the large symmetric orbit for $\omega = 1.8$ is shown in Fig. 4(b). As ω is further decreased, large symmetric orbit with higher torsion numbers, characterizing the average rotation numbers of the nearby orbits [4,5], appear successively. As examples, the phase portraits of the large symmetric orbits for $\omega = 0.85$ and 0.55 are shown in Figs. 4(c) and (d). Note that the large symmetric orbits with higher torsion numbers have an increasing number of loops. Furthermore, each large symmetric orbit becomes unstable through a symmetry-breaking PF bifurcation. Consequently, a pair of asymmetric orbits with broken symmetry appears. As an example, see the phase portrait of an asymmetric orbit for $\omega = 1.63$ in Fig. 4(e). Then, the asymmetric orbits with broken symmetry undergo period-doubling cascades, as shown in Fig. 4(a). Note that all these bifurcation behaviors are essentially the same as those in the single-well Duffing oscillator [4,5].

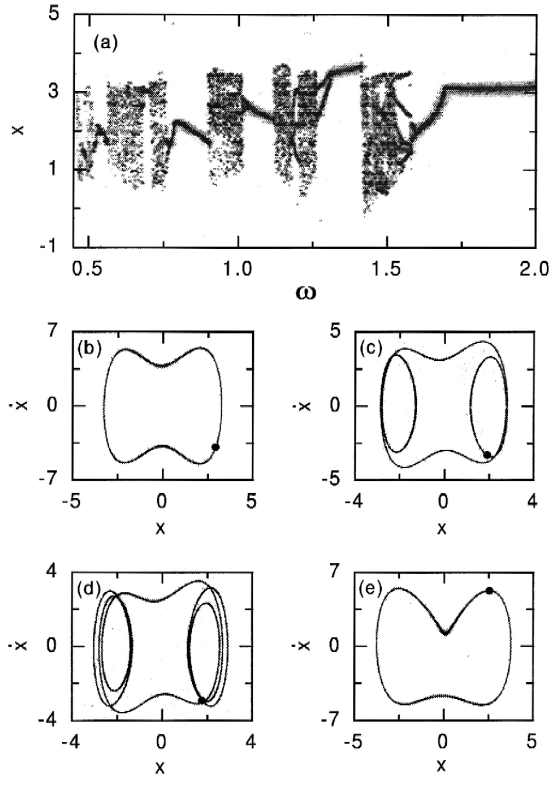

Fig. 4. Dynamical behavior after the dynamic stabilization. A bifurcation diagram of the Poincaré maps obtained with decreasing frequency ω for $A = 10$ is shown in (a). Phase flows (solid lines) and Poincaré maps (circles) of large symmetric orbits for $\omega = 1.8$, 0.85, and 0.55 are also given in (b), (c), and (d), respectively. Note that the large symmetric orbits with higher torsion numbers have an increasing number of loops. Furthermore, each symmetric orbit becomes unstable via a PF bifurcation, giving rise to a pair of asymmetric orbits. As an example, the phase portrait of an asymmetric orbit for $\omega = 1.63$ is given in (e). Then the asymmetric orbits with broken symmetry undergo period-doubling cascades, as shown in (a).

Finally we would like to mention that similar dynamic stabilization occurs in many other driven nonlinear dynamical systems. The best-known example is the inverted pendulum with a vertically-oscillating suspension point [18]. The inverted state, corresponding to the vertically-up configuration, was found to become stabilized via a reverse subcritical PF bifurcation [19]. The dynamic stabilization was also observed in the directly-driven pendulum [20]. Furthermore, such dynamic stabilization has its analog in the parametrically and directly driven sine-Gordon systems, which produce stable π-kink propagation [21–23].

In conclusion we experimentally investigated the dynamic stabilization of the unstable symmetric orbit, arising from the unstable equilibrium point of the potential, in the analog electronic circuit of the double-well Duffing oscillator. As the amplitude of the driving force increases through a threshold value, the unstable symmetric orbit was found to become stable via a reverse supercritical PF bifurcation by absorbing a pair of stable asymmetric orbits. The experimental results on the dynamic stabilization were confirmed and complemented the results of the numerical study quite well. After the dynamic stabilization, the double-well Duffing oscillator exhibits the

single-well-like behaviors, because the central potential barrier has no significant effect on the motion of the system. We also suggest that such dynamic stabilization is a generic property of driven nonlinear systems with humped potentials which provide both the stable and unstable equilibrium points.

Acknowledgements

This work was supported from the interdisciplinary research program of the Korea Science and Engineering Foundation under grant No. 1999-2-112-004-3 and the program of Ajou University Common Facility Laboratory.

References

[1] E.N. Lorentz, J. Atoms. Sci. 20 (1963) 130.
[2] G.L. Baker, J.P. Gollub, Chaotic Dynamics, Cambridge University Press, Cambridge, 1990.
[3] T. Kurz, W. Lauterborn, Phys. Lett. A 37 (1988) 1029.
[4] U. Parlitz, W. Lauterborn, Phys. Lett. A 107 (1985) 351.
[5] U. Parlitz, Int. J. Bif. Chaos 3 (1993) 703.
[6] P.J. Holmes, Philo. Trans. R. Soc. London Ser. A 292 (1979) 419.
[7] F.C. Moon, P.J. Holmes, J. Sound Vib. 65 (1979) 275.
[8] F.C. Moon, G.-X. Li, Phys. Rev. Lett. 55 (1985) 1439.
[9] F.T. Arecchi, F. Lisi, Phys. Rev. Lett. 49 (1982) 94.
[10] H. Ishii, H. Fujisaka, M. Inoue, Phys. Lett. A 116 (1986) 257.
[11] Y.H. Kao, J.C. Huang, Y.S. Gou, Phys. Rev. A 35 (1987) 5228.
[12] C.S. Wang, Y.H. Kao, J.C. Huang, Y.S. Gou, Phys. Rev. A 45 (1992) 3471.
[13] W. Szemplinska-Stupnicka, J. Rudowski, Chaos 3 (1993) 375.
[14] M. Lakshmanan, K. Murali, Chaos in Nonlinear Oscillators, World Scientific, Singapore, 1996.
[15] M.C. Cross, P.C. Hohenberg, Rev. Mod. Phys. 65 (1993) 851.
[16] S.-Y. Kim, Y. Kim, Phy. Rev. E 61 (2000) 6517.
[17] J. Guckenheimer, P. Holmes, Nonlinear Oscillations, Dynamical Systems, and Bifurcations of Vector Fields, Springer, Berlin, 1983.
[18] P.L. Kapitza, in: D. Ter Haar (Ed.), Collected Papers of P.L. Kapitza, Pergamon, London, 1965, p. 714.
[19] S.-Y. Kim, B. Hu, Phys. Rev. E 58 (1998) 3028, and references therein.
[20] J. Miles, Phys. Lett. A 133 (1988) 295.
[21] V. Zharnitsky, I. Mitkov, M. Levi, Phys. Rev. B 57 (1998) 5033.
[22] Y.S. Kivshar, N. Grønbech-Jensen, M.R. Samuelsen, Phys. Rev. B 45 (1992) 7789.
[23] V. Zharnitsky, I. Mitkov, N. Grønbech-Jensen, Phys. Rev. E 58 (1998) 52.